Mechanism of N-2 Reduction to NH3 by Aqueous Solvated Electrons

ARTICLE *in* THE JOURNAL OF PHYSICAL CHEMISTRY B · DECEMBER 2013

Impact Factor: 3.3 · DOI: 10.1021/jp406535p · Source: PubMed

4 AUTHORS, INCLUDING:

Robert J. Hamers
University of Wisconsin–Madison
387 PUBLICATIONS **17,304** CITATIONS

THE JOURNAL OF PHYSICAL CHEMISTRY B

Article

pubs.acs.org/JPCB

Mechanism of N_2 Reduction to NH_3 by Aqueous Solvated Electrons

Jeffrey R. Christianson, Di Zhu, Robert J. Hamers, and J. R. Schmidt*

Department of Chemistry, University of Wisconsin-Madison, Madison, Wisconsin 53706, United States

Supporting Information

ABSTRACT: Recently a novel approach to the photocatalytic reduction of molecular nitrogen under ambient conditions was reported in which hydrated electrons generated from ultraviolet illumination of diamond served as the reducing agent [Zhu, D.; Zhang, L.; Ruther, R. E.; Hamers, R. J. Photo-Illuminated Diamond as a Solid-State Source of Solvated Electrons in Water for Nitrogen Reduction. *Nat. Mater.* 2013, *12*, 836−841]. This surprising reduction of N_2 by aqueous solvated electrons is absent from the vast existing radiolysis literature and thus has little mechanistic precedent. In this work, a combination of experimental and computational approaches is used to elucidate the detailed molecular-level mechanistic pathway from nitrogen to ammonia. A variety of approaches, including electronic structure calculations, molecular dynamics simulations, kinetic modeling, and pH-dependent experimental measures of NH_3 and competing H_2 production, implicate a hydrogen atom addition mechanism at early reduction steps and sequential protonation/direct reduction by a solvated electron at later steps, thus involving both *direct* and *indirect* reactions with solvated electrons. This work provides a framework for understanding the possible application of solvated electrons as energetic reducing agents for chemically inert species under mild conditions.

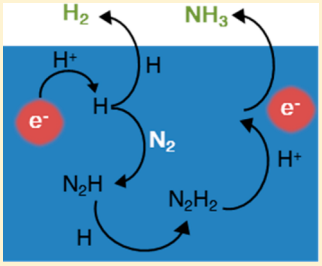

INTRODUCTION

Reduction of molecular nitrogen is extremely challenging due to its stability and chemical inertness.[1,2] Nonetheless, reduction of N_2 (and similarly stable and challenging CO_2) has attracted considerable attention due to the significant associated technological payoff. Although reduction of both N_2 and CO_2 are known to occur via a variety of different processes,[2,3] these processes often require complex biological enzymes,[4−9] harsh conditions (e.g., the Haber−Bosch process[10]), or inefficient electrochemical[3,11−13] and/or homo-[2,3,14] or heterogeneous[10,15] catalytic approaches.

Photocatalysis provides an alternative and particularly intriguing method for the reduction of inert species under ambient conditions. For reduction of N_2 in particular, this approach was first reported and subsequently improved using various modified forms of TiO_2.[16−23] In general, photoreduction of N_2 at surfaces is inefficient due to a combination of factors including weak adsorption of the inert reactant onto the surface under ambient conditions, the multielectron nature of the pathways to energetically accessible intermediates, and reoxidation of the intermediates and product by the holes in the deep-lying valence band of TiO_2 and other commonly used semiconductors.[24] Recently, Zhu, Hamers, and co-workers demonstrated the ability to reduce N_2 to NH_3 using hydrogen-terminated diamond as a source of photoemitted, and subsequently solvated, electrons.[25] Because hydrogen-terminated diamond has a negative electron affinity (NEA), the conduction band lies above the vacuum level,[26] and the main problems encountered with TiO_2 can be avoided; that is, while reduction via simple *photoexcitation* of the TiO_2 requires N_2 adsorption (along with associated ammonia reoxidation), *photoemission* occurs when hydrogen-terminated diamond is illuminated under deep ultraviolet (UV) light, eliminating the need for N_2 adsorption onto a solid surface and thereby minimizing product oxidation when appropriately coupled to an oxidation half-cell. Furthermore, the conduction band of diamond in water lies at a reduction potential of about −5 V versus that of the normal hydrogen electrode (NHE). Thus, in aqueous solution, the illuminated diamond serves as a source of high energy hydrated electrons capable of reducing N_2. While the yield is currently small (∼1−10 μg), reduction of N_2 (as opposed to nitrogen-containing impurities) by photoemission was confirmed by isotope-labeled studies.[25]

The initial proof-of-concept studies of Zhu et al. demonstrated both formation of solvated electrons and reduction of N_2 to NH_3 but did not determine the mechanistic pathway leading to ammonia. Furthermore, while the existing radiolysis literature contains a vast number of known reactions of the solvated electron, reactions involving N_2 are completely absent![27] Thus, the lack of a mechanistic hypothesis hinders both the prospects for optimization of the system as well as possible extensions to other challenging solution-phase reductions. In the present manuscript, a combination of experimental and computational techniques is used to elucidate the detailed mechanistic pathway leading from solvated electron to ammonia in N_2-saturated aqueous solution. This system serves as a convenient case study for reduction of inert species, since reduction leads to a single primary product (ammonia), in contrast to the reduction of other inert species such as CO_2 where multiple reduced products may be isolated.[3] In particular, two key fundamental questions are addressed: (1) Does the solvated electron directly reduce N_2 (aq) to N_2^- (aq),

Received: July 2, 2013
Revised: December 2, 2013
Published: December 9, 2013

   dx.doi.org/10.1021/jp406535p | *J. Phys. Chem. B* 2014, 118, 195−203

or does it first reduce some other aqueous species? (2) With what other processes does the desired reduction compete?

In considering the plausible mechanisms of N_2 reduction by solvated electrons, it is profitable to first consider previously determined or postulated mechanisms of N_2 reduction under other conditions. In the realm of heterogeneous catalysis, the Haber–Bosch process relies on both harsh conditions and a solid catalyst to dissociatively adsorb both N_2 and H_2; ammonia is then built from its atomic building blocks.[28,29] Since similar direct dissociation of N_2 via a solvated electron is nearly inconceivable, the rate-limiting step must instead be *activation* of the N–N triple bond; this is demonstrated by the strongly unfavorable redox potential of converting N_2 to N_2H (−3 V), which, in conjunction with subsequent steps, leads to an overall favorable 6 electron reduction potential (+ 0.55 V).[2,15]

Rather than cleaving the N–N bond, inorganic homogeneous catalysts begin the reduction process by weakening the bond for attack by a hydrogen source.[2,15] Similarly, one may hypothesize that the solvated electron may directly add to an antibonding π^* orbital of the N_2 molecule to yield N_2^-, thus activating the bond for further reduction. Although N_2 has a strongly unfavorable electron affinity in the gas phase, a crude estimate shows that this may be overcome via strong solvation of the nascent anion.[30] In enzymatic reactions, a strong coupling between electron transfer (ET) and proton transfer has been observed,[5,31] potentially even involving concerted proton-coupled ET (PCET). A similar mechanism could be conjectured in the present case, with the solvated electron and a water molecule serving as the electron and proton donors, respectively. While theoretical studies show that electrochemical N_2 reduction may occur via a dissociative mechanism at the electrode surface, depending on the metal used for the electrode,[32,33] a hydrogen atom addition (HAA) may be likely in many cases as well,[11] where protons are first reduced at the cathode to H atom before adding to the N_2. Note that it is well known that hydrated electrons react rapidly with protons and very slowly with water in aqueous solution to form hydrogen atoms.[27,34] On the basis of the prior relevant mechanistic data under these diverse conditions, ET, PCET, and HAA are considered here to be the most likely candidates for reduction of N_2 by solvated electrons.

We report here a comprehensive investigation into these possible mechanisms that implicates HAA at early reduction steps and sequential protonation/ET at later steps as the predominant pathway leading to ammonia. A new set of experiments are performed using an aqueous KI solution as a simpler and "cleaner" source of photoemitted hydrated electrons[35] (as compared to hydrogen-terminated diamond). This experimental setup confirms the contribution of *bulk* hydrated electrons to the reduction by removing any surface-dependent reactions and also allows for a study of the pH dependence of the reaction (which, in the case of diamond, could be complicated by pH-dependent changes in surface potentials or changes in the surface termination[36,37]). For the first time, the associated (and competing) H_2 yield is also observed. A conclusive mechanistic pathway is elucidated from this new set of experiments in conjunction with a diverse set of computational approaches involving electronic structure calculations, molecular dynamics (MD) simulations, and kinetic modeling.

METHODS

Experimental Section. A sample solution (10 mL) was prepared from 18.2 MΩ water and 0.1 mmol KI buffered by a Na_2HPO_4–NaH_2PO_4 system at the indicated pH with a total concentration of 8 mM. For pH 3 and 4 samples, H_3PO_4 was also added to adjust the pH. Then the sample solution, contained in a quartz vessel, was degassed using a vacuum line, followed by 50 sccm N_2 (99.9999999% purity) purging for 3 h to ensure a saturated solution for the photochemical reaction. All chemicals involved are in 99.99% trace metal basis purity. Photochemical experiments were performed using a high-pressure mercury lamp (Driel Instrument, model 66921), located approximately 10 in. from the samples, for typically 11 h. A water-absorptive filter was used to eliminate infrared (IR) radiation and UV radiation below 200 nm. The production of ammonia was measured using a high-performance ammonia ion selective electrode (Orion 9512HPBNWP). Gas-phase products, especially hydrogen gas, were determined by gas chromatography–thermal conductivity detection (GC-TCD) (Shimadzu GC-8A), with N_2 as the carrier gas. A colorimetric method[38] was used to measure the iodine (in the form of triiodide) concentration; the ultraviolet–visible (UV–vis) spectrum of the sample solution was taken right after reaction using a Shimadzu 2401PC UV–vis spectrophotometer. The absorbance at 351 nm was calibrated with known concentration samples as standards. Blank tests, including a dark control and an argon purging control (replacing N_2 with Ar), were conducted to rule out potential false results from contamination.

Kinetic Model. To perform a kinetic analysis of the known and possible reactions in solution, the Gepasi software package[39] was used to model the dynamics of a set of the most important (and well-characterized) reactions that are known to occur in the hydrated electron solution, taken from Table 2 in the review on solvated electron kinetics by Buxton et al.[27] Every reaction with a reported reliable measurement was considered. However, the extremely slow reaction of H atoms with water to produce H_2 has been significantly revised since Buxton's review, and the more recent rate constant for this reaction (4.4×10^{-5} M^{-1} s^{-1}) was used.[34] Also, the reaction of the buffer $H_2PO_4^-/HPO_4^{2-}$ with solvated electron to produce H atom was included.[27] In addition, no reactions involving O_2^{2-} were reported in this review, but by a Gaussian-4 (G4) and polarizable continuum model (PCM) thermodynamic analysis described below, O_2^{2-} reacts very exothermically with water to form HO_2^- and OH^- ($\Delta H_r = -20$. kcal/mol, $\Delta H_{r,gas} = -137$ kcal/mol). Thus, it is assumed that O_2^{2-} reacts with water with a diffusion-limited rate constant ($k_{diff} = 3 \times 10^{10}$ M^{-1} s^{-1}).

To estimate the concentration of solvated electron in solution, the rate of production of solvated electron is estimated from the experimental setup ($I^- + h\nu \rightarrow I + e^-$, with a first-order rate constant of $k_{prod} = 4 \times 10^{-6}$ s^{-1}). This rate constant was obtained by first integrating the irradiance of the light source[40] over the wavelengths above which the glass is transparent and below which electrons will be detached from iodide (200–254 nm) and then multiplying by the cross-section of the reaction vessel (12.8 cm^2) and the quantum efficiency (QE) of creating solvated electrons from iodide. The measured QE of 0.3 (at 248 nm) was assumed for all wavelengths since the QE increases only modestly to 0.5 by 193 nm.[41] The transmittance is expected to be less than 10^{-4}, on

dx.doi.org/10.1021/jp406535p | J. Phys. Chem. B 2014, 118, 195–203

the basis of the high molar absorptivity (885 $M^{-1}cm^{-1}$),[41] path length (2.5 cm), and iodide concentration (0.010 M); thus, it is assumed that all of the photons between 200 and 254 nm are absorbed by the sample. The value used for the quantum yield of solvated electrons includes primary geminate recombination,[41] but a rate for secondary recombination due to diffusion of iodine atoms and solvated electrons in solution must be considered. Since it is a radical reaction, it is reasonable to assume that this rate is diffusion-limited ($I + e^- \rightarrow I^-$; $k_{rec} = k_{diff}$). A comprehensive list of all reactions used in the kinetic model and their corresponding rate constants is provided in the Supporting Information.

The initial concentrations of all species were set to zero except water (55.5 M, fixed), H^+ and OH^- (fixed according to the appropriate pH), $H_2PO_4^-$ and HPO_4^{2-} (set to the buffer concentration at the appropriate pH), O_2 (100 nM, a reasonable upper bound for the amount present in the degassed water), I^- (0.01 M), and N_2 (0.6 mM). Once the appropriate set of reactions with N_2 were added, the Gepasi program was used to integrate the set of coupled differential equations over 11 h.

Gas-Phase Thermochemistry. Gas-phase transition states were located using density functional theory (DFT) with the ωB97X-D[42] functional with a 6-311++G(d,p) basis set as implemented in the Gaussian 09 software package.[43] The transition states were verified as saddle points via a frequency analysis. The one imaginary frequency was followed using the intrinsic reaction coordinate (IRC) method to verify that the two minima connected by the saddle point were the reactant and product states. The activation and reaction energies were then determined from single point calculations of the stationary points using CCSD(T) in conjunction with the triple-ζ correlation-consistent Dunning-style basis set augmented with diffuse functions (aug-cc-pVTZ). Free energies were obtained from frequency calculations of the stationary points, also at the CCSD(T)/aug-cc-pVTZ level of theory; however, the change in the gas-phase translational entropy was subtracted out and replaced by the cratic entropy (~4R) to estimate the solution-phase entropy change.[44,45] Where noted, the Gaussian-4 (G4) composite method[46] as implemented in Gaussian 09 was used to estimate thermochemical data, and enthalpies of solvation were estimated using the PCM.[47] For the latter calculations, DFT was used with the B3LYP functional and the 6-311++G(d,p) basis set.

Marcus Theory. Marcus theory[48,49] was used to estimate the barrier for ET from solvated electron to N_2 to form N_2^-(aq). The details have been laid out numerous times before;[48−50] discussed here are the important aspects for the current application of Marcus theory. Of particular importance is the fact that in this case, the electron donor is a solvated electron and is therefore not present in the product diabatic state. Hence the two diabatic states are $N_2\cdots e^-$ and N_2^-.

The difference in the internal energy between the two diabatic states is simply the electron affinity A of N_2. It is estimated that $A = -61$ kcal/mol (Bauer crudely estimates that $A \geq -63$ kcal/mol[30] from experimental data). The solvent interacts with each state in a way that depends on the solvent configuration, whose coordinates can be represented by a collective variable ξ. The reaction coordinate $\Delta\epsilon(\xi)$ is a collective solvent "energy gap" coordinate which is chosen to reflect the fact that the ET is driven by solvent fluctuations that provide stable solvation of the product state. It is often reasonable to assume linear solvent response to perturbations about the equilibrium, which gives rise to a simple expression for the activation free energy in terms of the free energy of reaction and the reorganization energy.[49−52] However, assuming linear solvent response may not be a good approximation in the case under current investigation where the electron donor is an electron with no associated nucleus; that is, the product state contains only one cavity in the solvent, whereas the reactant state contains two. For this reason, the free energy curves of the diabatic states were estimated along the entire reaction coordinate using biased sampling.

To generate the free energy as a function of the reaction coordinate, the solvent was considered explicitly, and Marcus theory was used to interpret a series of MD simulations. The simple point charge (SPC) water model[53] was used to describe the solvent; the Lennard-Jones (LJ) parameters for N_2 placed on the nitrogen atoms were taken from the all-atom transferable potentials for phase equilibria (TraPPE) force field[54] and used to describe the nitrogen−water interaction using the geometric mean of the individual parameters for the mixed parameters. For N_2^-, the same LJ parameters were used as for N_2, and a partial charge of −0.5 was placed on each N atom. The pseudopotential developed by Schnitker and Rossky[55] was used in its corrected form[56,57] to describe the electron−water interaction. The solvated electron was treated using a path integral approach[58] where the electron is represented by a closed ring composed of a number P of classical beads. Convergence with respect to the number of beads of the electron−oxygen and electron−hydrogen radial distribution functions and the electron radius of gyration was achieved by 200 beads, and the results were identical within statistical uncertainty to the quantum results presented previously,[56] so $P = 200$ was used. Once the solvated electron−water system had been equilibrated, a representative configuration of the electron beads was taken and used for the Marcus theory simulations, with the positions of the beads fixed. This was done for several configurations with negligible changes in the activation barrier, demonstrating that sampling over additional configurations of the electron beads is unnecessary. The electron−nitrogen interaction was neglected because for a given calculation of the ET barrier, the electron−nitrogen distance was fixed during the course of the simulation.

To determine a reasonable range of distances over which the N_2 and solvated electron could interact, a crude N_2−electron repulsive potential was used to compute a potential of mean force (PMF) for separating the two species. Details are provided in the Supporting Information.

As validation that these particular models for the electron−water and the N_2^-−water interactions will give a reasonable estimate of the solvation effects in the ET reaction, the difference in hydration enthalpy between the N_2^- and solvated electron is considered. The experimental value for the hydration enthalpy of the solvated electron is about −30 to −34 kcal/mol.[59,60] While no such corresponding value for N_2^- exists, it is reasonable to assume that it should be in the same range as that of a medium-sized halide (about −70 to −90 kcal/mol),[61] significantly less negative than that of OH^- (about −120 kcal/mol).[61] Given that both experimental and theoretical methods for determining ion enthalpies of hydration are questionable, the *relative* value for N_2^- compared to solvated electron is much more reliable. Experimental values for $\Delta H_{hyd}(e^-) - \Delta H_{hyd}(OH^-)$ and $\Delta H_{hyd}(e^-) - \Delta H_{hyd}(I^-)$ are 86 and 33 kcal/mol, respectively.[62] The present theoretical model's prediction for $\Delta H_{hyd}(e^-) - \Delta H_{hyd}(N_2^-)$ is 59 kcal/

dx.doi.org/10.1021/jp406535p | J. Phys. Chem. B 2014, 118, 195−203

mol, which reasonably lies between the two values. While less reliable absolute calculated values for $\Delta H_{hyd}(e^-)$ and $\Delta H_{hyd}(N_2^-)$ may indicate oversolvation in each case (−58 kcal/mol and −117 kcal/mol, respectively), the reasonable relative hydration value indicates that the ET barrier will be reasonably predicted to the desired accuracy, given the extremely high barrier predicted (see Results and Discussion sections).

Biased sampling was used so that solvent configurations all along the reaction coordinate were sampled. This was done by scaling the potential due to the nitrogen−electron system between the reactant and product diabatic states, similar to the procedure that Kuharski et al. used for modeling aqueous ferrous−ferric ET.[52] Details and a typical set of free energy curves are provided in the Supporting Information.

All of the MD simulations were run using a version of TINKER 5.0[63] that was locally modified to incorporate the ability to treat the electron using the path integral approach. Each simulation was run for 150 ps (following 50 ps of equilibration) with a 1.0 fs time step in the number−volume−temperature (*NVT*) ensemble at 298 K at the appropriate density for pure water (N = 216 water molecules in a cubic box with sides of length 18.6258 Å, corresponding to 1.00 g/cm^3). Periodic boundary conditions were applied with nonelectrostatic interactions cut off at 9.0 Å. Electrostatic interactions were treated with the particle mesh Ewald (PME) summation with tin foil boundary conditions and a uniform background charge.[64] The Ewald cutoff for real space interactions was 9 Å, and the PME summation used a 30 × 30 × 30 charge grid and 8th-order B-spline interpolation. Snapshots along the trajectory were saved every 100 fs, and the appropriate property was averaged over all snapshots.

The rate constant k for ET was calculated from the activation free energy ($\Delta G^{\ddagger}$) using[65]

$$k = \frac{2\pi}{\hbar} V^2 (4\pi\lambda k_B T)^{-1/2} \exp[-\beta \Delta G^{\ddagger}]$$

where V is the electronic coupling between the reactant and product states and is generously taken to be 10 meV to provide an upper bound for the estimated rate. In this expression for parabolic free energy curves, $\lambda = G_2(x_1) - G_1(x_1) = G_1(x_2) - G_2(x_2)$ is the reorganization energy, where $G_i(x_j)$ is the free energy of diabatic state i at the location along the reaction coordinate where the free energy of diabatic state j is a minimum. In the case where the curves are not parabolic, these two expressions are not necessarily equivalent. The expression that returned the smallest value of λ was used, so as to provide an upper bound for the rate constant. For the system presented here, the values differed by up to a factor of 4, corresponding to a difference of only a factor of 2 in the predicted rate, which is a trivial difference compared to the order-of-magnitude estimate obtained.

Preliminary results for the PCET barrier were calculated using the two-dimensional (2D) generalization of Marcus theory of Kobrak and Hammes-Schiffer for an atomistic treatment of the solvent.[66] However, it was assumed that proton transfer in the presence of the $N_2\cdots e^-$ complex was unimportant (since N_2H^+ is unlikely to form in N_2-saturated water), resulting in a simpler sampling of the potential energy surfaces. In the 2D generalization of Marcus theory, 2 collective solvent coordinates are used to describe the reaction coordinate, one for ET and one for proton transfer. The proton transfer coordinate was approximated to be parabolic, while the ET coordinate was sampled using the same biasing potential used for ET.

RESULTS

Under UV illumination of the N_2-saturated aqueous KI solution, reduction of N_2 gas to NH_3 was observed in addition to production of hydrogen gas and the oxidized iodide in the form of molecular iodine. The observed yields of NH_3, H_2, and I_2 are presented in Table 1 for several pH values ranging from 2 to 8. Throughout this manuscript, we refer to the product "yield" as the absolute amount produced under the experimental conditions and reaction times reported in the Methods section, consistent with the prior work of Zhu et al.[25] Higher pH conditions were not considered due to the dominance of the disproportionation reaction of I_2 with OH^- under basic conditions.[67] The majority of the reduced product is H_2, accounting for most of the electrons lost by the oxidized I^-. Ammonia, by contrast, is a minor product with smaller yields than previously reported for the reduction by photoemitted electrons from diamond; this may be due to a higher *local* solvated electron concentration induced in the vicinity of the diamond surface, potentially opening second-order (2 electron) reduction pathways. The good agreement between the measured I_2 yield and the expected I_2 yield (based on the measured H_2 and NH_3 yields) demonstrates that the majority of reduced products have been identified and quantified. On the basis of the experimental setup described above and the observed I_2 yield, we estimate that the quantum yield (fraction of photons that result in a solvated electron that produces NH_3 or H_2) at pH 7 is 4×10^{-3}. Since the quantum yield of solvated electrons is 0.3, this indicates that the vast majority of solvated electrons ultimately recombine (directly or indirectly) with I atoms.

Table 1. Observed pH Dependence of NH_3 and H_2 Yields (nmol) Compared to I_2 Yield (nmol)

pH	NH_3 yield	H_2 yield	expected I_2 yield[a]	I_2 yield
2.0	<LD[b]	575	575	562
3.0	3.2	349	354	339
4.0	3.6	226	231	244
4.6	6.9	208	218	231
5.0	8.2	183	195	213
6.0	6.6	202	212	187
7.0	3.2	231	236	228
8.0	2.5	173	177	217

[a]The expected I_2 yield is the H_2 yield added to three-halves of the NH_3 yield. [b]Limit of detection (LD) is 2 nmol.

Because of the necessary activation of the inert N−N triple bond, the initial elementary reaction of N_2 is likely to be rate limiting and thus demands considerable attention. As discussed above, we anticipate that the most likely initial elementary step is one of the following:

$$N_2 + H \rightarrow N_2H \quad \text{(HAA)} \tag{1}$$

$$N_2 + e^- \rightarrow N_2^- \quad \text{(ET)} \tag{2}$$

$$N_2 + e^- + H_2O \rightarrow N_2H + OH^- \quad \text{(PCET)} \tag{3}$$

However, since the ammonia yields are currently very low, almost *any* thermodynamically favorable reaction that activates the N−N bond could be involved and should be considered;

dx.doi.org/10.1021/jp406535p | J. Phys. Chem. B 2014, 118, 195−203

even activation via oxidation by an O_2 derivative may be plausible, given trace oxygen remaining in the degassed solution (e.g., rate-limiting oxidation to nitrate followed by subsequent reduction to ammonia). We therefore also consider the reaction of N_2 with other low-concentration species that are generated by solvated electrons in water with nontrivial amounts of O_2 (e.g., hydroxyl radical and hydrogen peroxide). To systematically enumerate *all* possible mechanisms, a list of all potential species in solution was constructed. The associated reaction enthalpy of each species with N_2 was estimated from enthalpies of formation and solvation (see Tables S2−S4 in the Supporting Information), calculated using standard electronic structure methods (see Supporting Information for details on thermodynamic screening). Eight additional plausible reactions with favorable, or mildly unfavorable, enthalpies of reactions were found, involving reaction of N_2 with 5 different reactants (Table S1 in the Supporting Information). However, all of these additional reactions were eliminated based on a combination of factors (i.e., highly improbable transition states, reactant's high reactivity with water, or an estimated upper bound on the reactant's equilibrium concentration); see Supporting Information for details. We thus consider reactions 1−3 as the only plausible initial mechanistic steps.

Reaction 2 initially seems implausible due to the highly unfavorable gas-phase electron affinity of N_2, estimated by thermodynamics,[30] electron scattering,[68] and theoretical calculations[69] to be between 50 and 60 kcal/mol. However, it has been shown that strong intermolecular interactions can be used to trap N_2^- even in the gas phase,[70] and thus strong solvation of N_2^- in water may make this reaction thermodynamically feasible. Assuming that the free energy of solvation of N_2^- lies between that of O_2^- (about −80 kcal/mol)[30] and OH^- (about −100 kcal/mol),[71] and given that the solvation free energy of the electron is about −40 kcal/mol,[59,60] the solvent could stabilize the product of reaction 2 over its reactants by 40−60 kcal/mol, approximately sufficient to account for the unfavorable electron affinity. Thus, while N_2^- would certainly be a short-lived intermediate, subsequent reaction with water and/or protons would lead to more stable reduced species. PCET (reaction 3) then represents the extreme limit of *concerted* (rather than sequential) electron/proton transfer. We therefore consider all three potential reactions using a kinetic analysis.

The rates of the known reactions of solvated electron in aqueous solution[27,34] were used as input for a kinetic model whose resulting set of coupled differential equations was then integrated over the experimental UV illumination time. However, solution-phase rate constants for reactions 1−3 were still needed as input for the model. For reaction 1, the rate constant was estimated to be 930 M^{-1} s^{-1} from a gas-phase CCSD(T)/aug-cc-pVTZ calculation based on transition state theory (TST),[1]

$$k = \frac{k_B T}{h} e^{-\Delta G^{\ddagger}/k_B T}$$

where k_B is Boltzmann's constant, T is room temperature, h is Planck's constant, and $\Delta G^{\ddagger}$ is the free energy of activation which was adjusted to estimate the solution-phase (rather than gas-phase) loss of translational entropy. The solution-phase barrier and corresponding rate constant for reaction 2 were estimated within the context of Marcus theory,[48−50] where the solvent was described explicitly in MD simulations. The rate constant for ET (reaction 2) was estimated from the Marcus theory pseudo-first-order rate constant to be 4×10^{-6} s^{-1}. Note that this rate constant is an electronic rate for a given (fixed) geometry and ignores the fact that the probability of obtaining that two-body geometry is much less than unity. Thus, it is an upper bound for the actual rate constant, ignoring mass transport. The barrier and corresponding rate constant for reaction 3 was considered in a similar manner but as a proton-coupled ET within the 2D extension of Marcus theory developed by Hammes-Schiffer and co-workers.[66] Only H_2O and not H^+ (or H_3O^+) was considered as the PCET proton donor, since the latter reacts extremely rapidly (diffusion limited) with a solvated electron to produce H atom. Preliminary results using H_2O as the proton donor indicated that the PCET barrier and the corresponding rate constant are both qualitatively similar to those for ET, as might be expected since one high-energy penalty (adding an electron to N_2) is replaced by another (heterolytically cleaving a water O−H bond).

The activation free energies for these reactions are given in Table 2, along with the estimated yield of NH_3 resulting from the kinetic model, assuming that every reaction with N_2 ends in the desired product (and neglecting any reverse reaction). Comparing to the experimental yield at pH 7.0 of 3.2 nmol, reaction 1 (HAA) is the only feasible pathway, producing a yield near the same order of magnitude as (but considerably larger than) the experimental data, while ET exhibits negligible yields; this allows the elimination of direct ET and, because of the similar barriers, PCET processes as the initial reduction step.

Table 2. Free Energies of Activation (kcal/mol) and Estimated Ammonia Yields (nmol) at pH 7.0 from the Kinetic Model, for HAA and ET

rxn.	reactant	ΔG^{TS}	NH_3 yield[a]	equil. NH_3 yield[b]
1	H	13.4	360	4.6
2	e^-	24	2.3×10^{-7}	
	expt. NH_3 yield		3.2	

[a]Includes the activation barrier but excludes the reverse reaction. [b]Includes both the activation barrier and the reverse reaction, assuming a thermoneutral reaction.

However, while the HAA pathway is plausible, it does not provide a stable thermodynamic sink that can feed subsequent elementary steps. We thus consider the following two-step process,

$$N_2 + H \leftrightarrows N_2H \quad (1a)$$

$$N_2H + H \rightarrow N_2H_2 \quad (1b)$$

yielding an activated, thermodynamically stable, N_2H_2 intermediate that is presumably rapidly reduced to NH_3. Electronic structure calculations estimate that the free energy of 1a in the gas-phase is +8 kcal/mol (which compares well to an experimental *enthalpy* of reaction of +6 kcal/mol[72]). However, the dielectric constant of the solvent gives rise to a stabilization of the product estimated at ∼3 kcal/mol using PCM solvation. Explicit hydrogen bonding of N_2H with water will further stabilize the product; gas-phase calculations estimate that the strength of the hydrogen bond between N_2H and one water molecule is ∼5 kcal/mol. We thus assume an overall thermoneutral reaction, resulting in a rate constant for the reverse reaction of 930 M^{-1} s^{-1} as determined by detailed

dx.doi.org/10.1021/jp406535p | J. Phys. Chem. B 2014, 118, 195−203

balance. In contrast, reaction 1b is very exothermic ($\Delta H_r = -63$ kcal/mol from the G4 electronic structure calculations); therefore, N_2H_2 provides a stable thermodynamic sink for the further facile reduction to NH_3. This subsequent step is assumed to proceed with a diffusion-limited rate constant in the kinetic model; the result is shown in the last column of Table 2, with a predicted NH_3 yield of 4.6 nmol, quite close to the observed value of 3.2 nmol.

DISCUSSION

On the basis of these analyses, it appears likely that the mechanism for aqueous N_2 reduction to NH_3 by solvated electron proceeds by H atom addition through both N_2H and N_2H_2 intermediates. Note that this conclusion has been drawn from the kinetic model by neglecting any potential photochemical effects. The continuous illumination of the sample under the UV light may affect any intermediate along the reaction path from N_2 to NH_3. The most likely effect of the light seems to be photolysis of water from the deep UV light that is not absorbed by the quartz reaction vessel; most, but not all, of this has been filtered out by a water bath in front of the sample.

However, the H atom addition mechanism alone does not explain the experimental observation that the NH_3 yield decreases and eventually shuts off as the pH is decreased (see Table 1). Thus, the initial H addition to N_2 cannot be rate limiting at low pH. Otherwise, as the pH decreases, H concentration should increase (due to solvated electrons reacting with the increased number of protons), and production of N_2H_2 (and therefore NH_3) should also increase, in contrast to experimental observations.

A resolution comes from considering subsequent reduction steps involving expected partially reduced intermediates, such as diazene (N_2H_2) or hydrazine (N_2H_4), which also have been posited as intermediates in the photocatalytic reduction at semiconductor surfaces.[73] In particular, the latter is almost always protonated under the experimental conditions (pK_a = 8.0[69]), yielding $N_2H_5^+$. Electronic structure calculations estimate that the protonated species has a solution-phase electron affinity of approximately +3 kcal/mol, allowing for reaction with a solvated electron, and yielding a reduced neutral species, and eventually NH_3. In contrast, these same electronic structure methods suggest a substantial barrier to direct H atom addition to hydrazine (approximately 5 kcal/mol). Thus the predominant pathway for later reduction is expected to consist of *sequential* protonation and direct reduction by solvated electron. At low pH, this process will be hindered by the very low steady-state concentrations of solvated electron (since they rapidly react with protons), while at higher pH values (4–7), there are sufficient solvated electrons available such that these later steps are not rate-limiting. A similar argument could also be made for diazene (gas-phase barrier to H addition of 2 kcal/mol, solution-phase proton affinity of +6 kcal/mol, $N_2H_3^+$ solution-phase electron affinity of −72 kcal/mol) or for any other intermediates between N_2H_2 and NH_3 that are expected to have a high pK_a.

This conclusion is supported by the kinetic model. To incorporate this effect, N_2H_2 is assumed to react with solvated electrons with a diffusion-limited rate constant to produce NH_3 (although, in practice, this must occur via a series of elementary steps). Anywhere from one to four steps involving direct electron addition (as opposed to H atom addition) could be involved. Data for including both two and four direct ET steps are presented in Figure 1, and the general shape of the pH dependence is captured well in both cases. The discrepancies

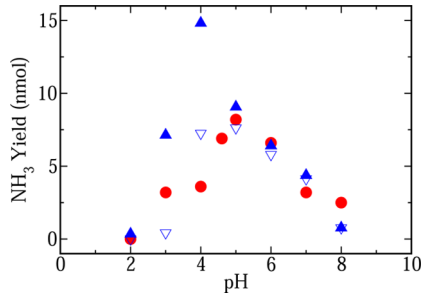

Figure 1. pH dependence of ammonia yield from the kinetic model with 2 (closed triangles, ▲) and 4 (open triangles, ▽) direct ET steps. Yields from experiment are shown in closed circles (●).

between the model and experiment are well within the uncertainties of the model, with the steady-state H atom concentration and the solution-phase exothermicity of reaction 1a as the two major sources of uncertainty in the results.

Reactions 1a and 1b both depend on the concentration of H atom, and so the NH_3 yield is essentially second order in H atom concentration. Thus, given the uncertainty of the rates used in the model, small errors in predicting H atom concentration (for example due to errors in approximating the rate of electron production or recombination or neglecting photolysis of water by very low-wavelength light) can easily explain the differences between predicted and observed NH_3 yields. On the basis of the reaction rates and species concentrations, reaction 1a can be assumed to be in quasi-equilibrium. As such, the model is *extremely* insensitive to the detailed solution phase hydrogen addition reaction barrier. For example, decreasing the rate constant by 2 orders of magnitude only decreases the ammonia yield by a factor of 2. However, the results are modestly influenced by estimates of the reaction free energy of reaction 1a and the resulting equilibrium. Overall, the experimental drops in yield at both high and low pH are well-described by the model's simple description of the competition between protons producing H atoms at high pH and solvated electrons necessary for later steps at low pH.

In contrast to the good agreement for NH_3 yields, the H_2 production is overestimated by the model at most pH values, from a factor of 4 at pH 7 to more than a factor of 30 at low pH (Figure 2). The increase in H_2 yield with pH values decreasing from 7, observed in Table 1, is easily understood by the known fast reaction of protons with solvated electrons to form H atoms which in turn react to form H_2.[27] At low pH, protons

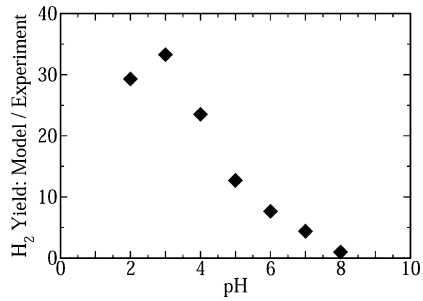

Figure 2. Ratio of H_2 yield predicted by the model to that observed experimentally as a function of pH.

dx.doi.org/10.1021/jp406535p | J. Phys. Chem. B 2014, 118, 195–203

(supplied by the buffer) compete more favorably with I atoms (recombination) for reaction with solvated electrons. (Although there are several processes by which H_2 can be produced, the H + H pathway is second-order in H atom and will therefore dominate at low pH.) Indeed, the kinetic model for I^- in pure water (no O_2, N_2, or buffer, but $[H^+]$ and $[OH^-]$ held fixed at the appropriate pH) indicates that H_2 production should increase by nearly 3 orders of magnitude from pH 8 to pH 2. However, the experimentally measured H_2 yield increases by less than a factor of 5 over the same range.

This discrepancy can be resolved by noting that I atoms can react with H_2 to form HI, as previously observed both in the gas phase[74] and in relatively high yields in a high-temperature aqueous environment.[75] Indeed, indirect recombination of solvated electrons with I atoms by first reacting with a proton has been postulated before.[68] Preliminary experiments demonstrate the feasibility of such a process for the present system; reacting saturated aqueous H_2 and I_2 under the photochemical conditions of this study (with the photolysis of I_2 to I) yields spectroscopic data consistent with I_2 converted to I^-, along with a corresponding drop in pH. Control experiments show no I^- in the absence of H_2. As such, while the exact mechanism is still debated,[76] it appears likely that H_2 product is being reoxidized under the current conditions. As a result, aqueous H^+ and I^- are formed, consuming H_2 and I_2, essentially serving to recombine the solvated electron with I atoms via a proton mediator. This accounts for the relatively small change in H_2 yield as a function of pH while still observing conservation of charge through comparison of the reduction and oxidation product yields in Table 1. The omission of these reactions also explains the large discrepancies between the model and the experimental H_2 yield at low pH values, where indirect recombination occurs in larger quantities due to the increased amounts of H_2 available. We also note that this indirect recombination is not included in our estimate of the quantum yield, which is therefore a lower bound due to undetected I_2.

CONCLUSIONS

Reduction of stable species, such as N_2, via solvated electrons presents interesting challenges and potential opportunities. The present work provides a first step toward a more fundamental understanding of the mechanism of these complex processes. Overall, it is found that reduction of N_2 to NH_3 occurs via a combination of initial direct H atom addition and subsequent sequential protonation/ET. The unique combination of these two reduction pathways, including both *direct* and *indirect* reactions with solvated electrons, leads to a characteristic pH dependence that has been verified by a combination of experimental and computational methods, along with detailed kinetic modeling. We conclude that the proposed mechanism, involving HAA at initial steps, and sequential protonation/direct reduction by solvated electrons at later steps, is the only plausible mechanism for N_2 reduction by aqueous solvated electrons.

Overall, this mechanism is likely quite similar to what would be expected in some electrochemical reductions of N_2 at electrode surfaces, depending on the metal used. However, because of the potentials involved, it is expected that the direct reduction of protons to H_2 would be a dominant side reaction. In particular, the extremely high local concentration of adsorbed H atoms at the electrode surface, coupled with the small amount of adsorbed N_2, would most likely lead to nearly exclusive production of H_2 over NH_3. In contrast, reduction by solvated electrons in bulk solution reduces the local H atom concentration and allows N_2 reduction to compete more favorably with H_2 production, although the latter is still the majority product. Thus, maximizing selectivity for the desired reduction over H_2 production seems to be one of the principle challenges for such solvated electron-mediated reductions in aqueous solution. This also suggests the potential promise of related reductions in electrochemically stable nonaqueous solvents, which may proceed via alternative pathways with increased selectivity and efficiency.

ASSOCIATED CONTENT

Supporting Information

Details of methods used for and results obtained from the thermodynamic screening. Further details of methods used for calculating N_2-solvated electron PMFs, along with a figure of representative PMFs. Further details of the biased sampling method used. Figure showing representative Marcus curves for the ET reaction. Figure showing reaction barrier as a function of N_2-solvated electron distance for the ET reaction. Tables of the 83 neutral and ionic species used for the thermodynamic screening and their calculated enthalpies of formation and solvation. Table containing rate constants used in the kinetic model. This material is available free of charge via the Internet at http://pubs.acs.org.

AUTHOR INFORMATION

Corresponding Author

*E-mail: schmidt@chem.wisc.edu.

Notes

The authors declare no competing financial interest.

ACKNOWLEDGMENTS

The computational studies reported here were partially supported by the University of Wisconsin Materials Research Science and Engineering Center under Award DMR-1121288 (J.R.C.). Experimental studies of N_2 reduction were supported by the National Science Foundation under Award DMR-1207281 (D.Z.). Computational resources were utilized from the Center for High Throughput Computing (CHTC)[77] and by National Science Foundation Grant CHE-0840494. J.R.S. is an Alfred P. Sloan Research Fellow. The authors also thank Prof. Gil Nathanson for many helpful discussions.

REFERENCES

(1) Chatt, J.; Dilworth, J. R.; Richards, R. L. Recent Advances in the Chemistry of Nitrogen Fixation. *Chem. Rev. (Washington, DC, U. S.)* **1978**, *78*, 589−625.

(2) Bazhenova, T. A.; Shilov, A. E. Nitrogen Fixation in Solution. *Coord. Chem. Rev.* **1995**, *144*, 69−145.

(3) Benson, E. E.; Kubiak, C. P.; Sathrum, A. J.; Smieja, J. M. Electrocatalytic and Homogeneous Approaches to Conversion of CO_2 to Liquid Fuels. *Chem. Soc. Rev.* **2009**, *38*, 89−99.

(4) Kim, J.; Rees, D. C. Nitrogenase and Biological Nitrogen Fixation. *Biochemistry* **1994**, *33*, 389−397.

(5) Burgess, B. K.; Lowe, D. J. Mechanism of Molybdenum Nitrogenase. *Chem. Rev. (Washington, DC, U. S.)* **1996**, *96*, 2983−3012.

(6) Eady, R. R. Structure−Function Relationships of Alternative Nitrogenases. *Chem. Rev. (Washington, DC, U. S.)* **1996**, *96*, 3013−3030.

(7) Eady, R. R. Current Status of Structure Function Relationships of Vanadium Nitrogenase. *Coord. Chem. Rev.* **2003**, *237*, 23−30.

(8) Jeoung, J.-H.; Dobbek, H. Carbon Dioxide Activation at the Ni,Fe-Cluster of Anaerobic Carbon Monoxide Dehydrogenase. *Science* **2007**, *318*, 1461−1464.
(9) Dobbek, H.; Gremer, L.; Meyer, O.; Huber, R. Crystal Structure and Mechanism of CO Dehydrogenase, a Molybdo Iron-Sulfur Flavoprotein Containing S-Selanylcysteine. *Proc. Natl. Acad. Sci. U.S.A.* **1999**, *96*, 8884−8889.
(10) Hardy, R. W. F. *A Treatise on Dinitrogen Fixation*; Wiley: New York, 1979; p 291−332.
(11) Murakami, T.; Nishikiori, T.; Nohira, T.; Ito, Y. Electrolytic Synthesis of Ammonia in Molten Salts under Atmospheric Pressure. *J. Am. Chem. Soc.* **2002**, *125*, 334−335.
(12) Murakami, T.; Nohira, T.; Araki, Y.; Goto, T.; Hagiwara, R.; Ogata, Y. H. Electrolytic Synthesis of Ammonia from Water and Nitrogen under Atmospheric Pressure Using a Boron-Doped Diamond Electrode as a Nonconsumable Anode. *Electrochem. Solid-State Lett.* **2007**, *10*, E4−E6.
(13) Marnellos, G.; Stoukides, M. Ammonia Synthesis at Atmospheric Pressure. *Science* **1998**, *282*, 98−100.
(14) Wang, S.; Lu, G. Q.; Millar, G. J. Carbon Dioxide Reforming of Methane to Produce Synthesis Gas over Metal-Supported Catalysts: State of the Art. *Energy Fuels* **1996**, *10*, 896−904.
(15) Shilov, A. E. Catalytic Reduction of Molecular Nitrogen in Solutions. *Russ. Chem. Bull.* **2003**, *52*, 2555−2562.
(16) Schrauzer, G. N.; Guth, T. D. Photocatalytic Reactions. 1. Photolysis of Water and Photoreduction of Nitrogen on Titanium Dioxide. *J. Am. Chem. Soc.* **1977**, *99*, 7189−7193.
(17) Dickson, C. R.; Nozik, A. J. Nitrogen Fixation via Photo-enhanced Reduction on p-Gallium Phosphide Electrodes. *J. Am. Chem. Soc.* **1978**, *100*, 8007−8009.
(18) Miyama, H.; Fujii, N.; Nagae, Y. Heterogeneous Photocatalytic Synthesis of Ammonia from Water and Nitrogen. *Chem. Phys. Lett.* **1980**, *74*, 523−524.
(19) Vettraino, M.; Trudeau, M.; Lo, A. Y. H.; Schurko, R. W.; Antonelli, D. Room-Temperature Ammonia Formation from Dinitrogen on a Reduced Mesoporous Titanium Oxide Surface with Metallic Properties. *J. Am. Chem. Soc.* **2002**, *124*, 9567−9573.
(20) Rao, N. N.; Dube, S.; Manjubala; Natarajan, P. Photocatalytic Reduction of Nitrogen over (Fe, Ru or Os) /TiO_2 Catalysts. *Appl. Catal., B* **1994**, *5*, 33−42.
(21) Ranjit, K. T.; Varadarajan, T. K.; Viswanathan, B. Photocatalytic Reduction of Dinitrogen to Ammonia over Noble-Metal-Loaded TiO_2. *J. Photochem. Photobiol., A* **1996**, *96*, 181−185.
(22) Litter, M. I.; Navío, J. A. Photocatalytic Properties of Iron-Doped Titania Semiconductors. *J. Photochem. Photobiol., A* **1996**, *98*, 171−181.
(23) Hoshino, K.; Kuchii, R.; Ogawa, T. Dinitrogen Photofixation Properties of Different Titanium Oxides in Conducting Polymer/Titanium Oxide Hybrid Systems. *Appl. Catal., B* **2008**, *79*, 81−88.
(24) Mozzanega, H.; Herrmann, J. M.; Pichat, P. Ammonia Oxidation over UV-Irradiated Titanium Dioxide at Room Temperature. *J. Phys. Chem.* **1979**, *83*, 2251−2255.
(25) Zhu, D.; Zhang, L.; Ruther, R. E.; Hamers, R. J. Photo-Illuminated Diamond as a Solid-State Source of Solvated Electrons in Water for Nitrogen Reduction. *Nat. Mater.* **2013**, *12*, 836−841.
(26) van der Weide, J.; Zhang, Z.; Baumann, P. K.; Wensell, M. G.; Bernholc, J.; Nemanich, R. J. Negative-Electron-Affinity Effects on the Diamond (100) Surface. *Phys. Rev. B: Condens. Matter Mater. Phys.* **1994**, *50*, 5803−5806.
(27) Buxton, G. V.; Greenstock, C. L.; Helman, W. P.; Ross, A. B. Critical Review of Rate Constants for Reactions of Hydrated Electrons, Hydrogen Atoms and Hydroxyl Radicals (OH/O^-) in Aqueous Solution. *J. Phys. Chem. Ref. Data* **1988**, *17*, 513−886.
(28) Bozso, F.; Ertl, G.; Grunze, M.; Weiss, M. Interaction of Nitrogen with Iron Surfaces: I. Fe(100) and Fe(111). *J. Catal.* **1977**, *49*, 18−41.
(29) Honkala, K.; Hellman, A.; Remediakis, I. N.; Logadottir, A.; Carlsson, A.; Dahl, S.; Christensen, C. H.; Nørskov, J. K. Ammonia Synthesis from First-Principles Calculations. *Science* **2005**, *307*, 555−558.
(30) Bauer, N. Theoretical Pathways for the Reduction of N_2 Molecules in Aqueous Media: Thermodynamics of N_2H_n. *J. Phys. Chem.* **1960**, *64*, 833−837.
(31) Siegbahn, P. E. M.; Westerberg, J.; Svensson, M.; Crabtree, R. H. Nitrogen Fixation by Nitrogenases: A Quantum Chemical Study. *J. Phys. Chem. B* **1998**, *102*, 1615−1623.
(32) Skulason, E.; Bligaard, T.; Gudmundsdottir, S.; Studt, F.; Rossmeisl, J.; Abild-Pedersen, F.; Vegge, T.; Jonsson, H.; Norskov, J. K. A Theoretical Evaluation of Possible Transition Metal Electro-Catalysts for N_2 Reduction. *Phys. Chem. Chem. Phys.* **2012**, *14*, 1235−1245.
(33) Howalt, J. G.; Bligaard, T.; Rossmeisl, J.; Vegge, T. DFT-Based Study of Transition Metal Nano-Clusters for Electrochemical NH_3 Production. *Phys. Chem. Chem. Phys.* **2013**, *15*, 7785−7795.
(34) Bartels, D. M. Comment on the Possible Role of the Reaction H + $H_2O \rightarrow H_2$ + OH in the Radiolysis of Water at High Temperatures. *Radiat. Phys. Chem.* **2009**, *78*, 191−194.
(35) Lian, R.; Oulianov, D. A.; Crowell, R. A.; Shkrob, I. A.; Chen, X.; Bradforth, S. E. Electron Photodetachment from Aqueous Anions. 3. Dynamics of Geminate Pairs Derived from Photoexcitation of Mono- vs Polyatomic Anions. *J. Phys. Chem. A* **2006**, *110*, 9071−9078.
(36) Garrido, J. A.; Nowy, S.; Hartl, A.; Stutzmann, M. The Diamond/Aqueous Electrolyte Interface: An Impedance Investigation. *Langmuir* **2008**, *24*, 3897−3904.
(37) Ristein, J.; Zhang, W.; Ley, L. Hydrogen-Terminated Diamond Electrodes. I. Charges, Potentials, and Energies. *Phys. Rev. E: Stat., Nonlinear, Soft Matter Phys.* **2008**, *78*, 041602.
(38) Wei, Y.-j.; Liu, C.-g.; MO, L.-p. Ultraviolet Absorption Spectra of Iodine, Iodide Ion and Triiodide Ion. *Spectrosc. Spectral Anal. (Beijing, China)* **2005**, *25*, 86−88.
(39) Mendes, P. GEPASI: A Software Package for Modelling the Dynamics, Steady States and Control of Biochemical and Other Systems. *CABIOS, Comput. Appl. Biosci.* **1993**, *9*, 563−571.
(40) Newport. Oriel Product Training: Spectral Irradiance. http://assets.newport.com/webdocuments-en/images/light_sources.pdf (accessed September 2012).
(41) Sauer, M. C.; Crowell, R. A.; Shkrob, I. A. Electron Photodetachment from Aqueous Anions. 1. Quantum Yields for Generation of Hydrated Electron by 193 and 248 nm Laser Photoexcitation of Miscellaneous Inorganic Anions. *J. Phys. Chem. A* **2004**, *108*, 5490−5502.
(42) Chai, J.-D.; Head-Gordon, M. Long-Range Corrected Hybrid Density Functionals with Damped Atom—Atom Dispersion Corrections. *Phys. Chem. Chem. Phys.* **2008**, *10*, 6615−6620.
(43) Frisch, M. J.; Trucks, G. W.; Schlegel, H. B.; Scuseria, G. E.; Robb, M. A.; Cheeseman, J. R.; Scalmani, G.; Barone, V.; Mennucci, B.; Petersson, G. A. et al., *Gaussian 09*, Revision A.02; Gaussian, Inc.: Wallingford, CT, 2009.
(44) Buehler, R. E.; Staehelin, J.; Hoigne, J. Ozone Decomposition in Water Studied by Pulse Radiolysis. 1. HO_2/O_2^- and HO_3/O_3^- as Intermediates. *J. Phys. Chem.* **1984**, *88*, 2560−2564.
(45) Sehested, K.; Holcman, J.; Hart, E. J. Rate Constants and Products of the Reactions of e_{aq}^-, O_2^-, and H with Ozone in Aqueous Solutions. *J. Phys. Chem.* **1983**, *87*, 1951−1954.
(46) Curtiss, L. A.; Redfern, P. C.; Raghavachari, K. Gaussian-4 Theory. *J. Chem. Phys.* **2007**, *126*, 084108−084112.
(47) Tomasi, J.; Mennucci, B.; Cammi, R. Quantum Mechanical Continuum Solvation Models. *Chem. Rev. (Washington, DC, U. S.)* **2005**, *105*, 2999−3094.
(48) Marcus, R. A. On the Theory of Oxidation-Reduction Reactions Involving Electron Transfer. I. *J. Chem. Phys.* **1956**, *24*, 966−978.
(49) Marcus, R. A. Chemical and Electrochemical Electron-Transfer Theory. *Annu. Rev. Phys. Chem.* **1964**, *15*, 155−196.
(50) Zwickl, J.; Shenvi, N.; Schmidt, J. R.; Tully, J. C. Transition State Barriers in Multidimensional Marcus Theory. *J. Phys. Chem. A* **2008**, *112*, 10570−10579.

(51) Warshel, A. Dynamics of Reactions in Polar Solvents. Semiclassical Trajectory Studies of Electron-Transfer and Proton-Transfer Reactions. *J. Phys. Chem.* **1982**, *86*, 2218−2224.
(52) Kuharski, R. A.; Bader, J. S.; Chandler, D.; Sprik, M.; Klein, M. L.; Impey, R. W. Molecular Model for Aqueous Ferrous—Ferric Electron Transfer. *J. Chem. Phys.* **1988**, *89*, 3248−3257.
(53) Berendsen, H. J. C.; Postma, J. P. M.; van Gunsteren, W. F.; Hermans, J. *Intermolecular Forces*; Reidel: Dordrecht, Netherlands, 1981; p 331.
(54) Potoff, J. J.; Siepmann, J. I. Vapor−Liquid Equilibria of Mixtures Containing Alkanes, Carbon Dioxide, and Nitrogen. *AIChE J.* **2001**, *47*, 1676−1682.
(55) Schnitker, J.; Rossky, P. J. An Electron—Water Pseudopotential for Condensed Phase Simulation. *J. Chem. Phys.* **1987**, *86*, 3462−3470.
(56) Larsen, R. E.; Glover, W. J.; Schwartz, B. J. Comment on "An Electron-Water Pseudopotential for Condensed Phase Simulation" [J. Chem. Phys. **86**, 3462 (1987)]. *J. Chem. Phys.* **2009**, *131*, 037101−037102.
(57) Schnitker, J.; Rossky, P. J. Response to Comment on "An Electron-Water Pseudopotential for Condensed Phase Simulation" [J. Chem. Phys. **131**, 037101 (2009)]. *J. Chem. Phys.* **2009**, *131*, 037102−037101.
(58) Berne, B. J.; Thirumalai, D. On the Simulation of Quantum Systems: Path Integral Methods. *Annu. Rev. Phys. Chem.* **1986**, *37*, 401−424.
(59) Schwarz, H. A. Enthalpy and Entropy of Formation of the Hydrated Electron. *J. Phys. Chem.* **1991**, *95*, 6697−6701.
(60) Han, P.; Bartels, D. M. Reevaluation of Arrhenius Parameters for $H + OH^- \rightarrow (e^-)_{aq} + H_2O$ and the Enthalpy and Entropy of Hydrated Electrons. *J. Phys. Chem.* **1990**, *94*, 7294−7299.
(61) Marcus, Y. A Simple Empirical Model Describing the Thermodynamics of Hydration of Ions of Widely Varying Charges, Sizes, and Shapes. *Biophys. Chem* **1994**, *51*, 111−127.
(62) Shiraishi, H.; Sunaryo, G. R.; Ishigure, K. Temperature Dependence of Equilibrium and Rate Constants of Reactions Inducing Conversion between Hydrated Electron and Atomic Hydrogen. *J. Phys. Chem.* **1994**, *98*, 5164−5173.
(63) Ponder, J. W., *TINKER: Software Tools for Molecular Design*, 5.0; Washington University School of Medicine: Saint Louis, MO, 2009.
(64) Frenkel, D.; Smit, B. *Understanding Molecular Simulation: From Algorithms to Applications*, 2nd ed.; Academic Press: San Diego, CA, 2002; pp 291−320.
(65) Closs, G. L.; Miller, J. R. Intramolecular Long-Distance Electron Transfer in Organic Molecules. *Science* **1988**, *240*, 440−447.
(66) Kobrak, M. N.; Hammes-Schiffer, S. Molecular Dynamics Simulation of Proton-Coupled Electron Transfer in Solution. *J. Phys. Chem. B* **2001**, *105*, 10435−10445.
(67) Sebők-Nagy, K.; Körtvélyesi, T. Kinetics and Mechanism of the Hydrolytic Disproportionation of Iodine. *Int. J. Chem. Kinet.* **2004**, *36*, 596−602.
(68) Schulz, G. J. Resonances in Electron Impact on Diatomic Molecules. *Rev. Mod. Phys.* **1973**, *45*, 423−486.
(69) Gianturco, F. A.; Schneider, F. A Bound-State CI Approach to Nitrogen Molecular Anions. *J. Phys. B: At., Mol. Opt. Phys.* **1996**, *29*, 1175.
(70) Skurski, P.; Simons, J. An Unstable Anion Stabilized in a Molecular Trap. *J. Phys. Chem. A* **2000**, *104*, 712−717.
(71) Marcus, Y. Thermodynamics of Solvation of Ions. Part 5. Gibbs Free Energy of Hydration at 298.15 K. *J. Chem. Soc., Faraday Trans.* **1991**, *87*, 2995−2999.
(72) Bozzelli, J. W.; Dean, A. M. O + NNH: A Possible New Route for NO_X Formation in Flames. *Int. J. Chem. Kinet.* **1995**, *27*, 1097−1109.
(73) Linnik, O.; Kisch, H. On the Mechanism of Nitrogen Photofixation at Nanostructured Iron Titanate Films. *Photochem. Photobiol. Sci.* **2006**, *5*, 938−942.
(74) Sullivan, J. H. Mechanism of the "Bimolecular" Hydrogen—Iodine Reaction. *J. Chem. Phys.* **1967**, *46*, 73−78.
(75) Castleman, A. W., Jr; Tang, I. N.; Munkelwitz, H. R. The Chemical States of Fission-Product Iodine Emanating into a High Temperature Aqueous Environment. *J. Inorg. Nucl. Chem.* **1968**, *30*, 5−13.
(76) Anderson, J. B. Potential Energy Surface for the Hydrogen—Iodine Reaction. *J. Chem. Phys.* **1994**, *100*, 4253−4255.
(77) Litzkow, M.; Livney, M.; Mutka, M. *Condor—A Hunter of Idle Workstations*; IEEE: New York, 1988.